A novel nanosilica/graphene oxide hybrid and its flame retarding epoxy resin with simultaneously improved mechanical, thermal conductivities, and dielectric properties†

Rui Wang[13], Dongxian Zhuo[12], Zixiang Weng[13], Lixin Wu[12*], Xiuyan Cheng[1], Yu Zhou[1], Jianlei Wang[1], Bowen Xuan[13]

[1]Key Laboratory of design and assembly of functional nanostructures, Fujian Institute of Research on the Structure of Matter, Chinese Academy of Sciences, Fuzhou 350002, China

[2]Fujian Provincial Key Laboratory of Nanomaterials, Fujian Institute of Research on the Structure of Matter, Chinese Academy of Sciences, Fuzhou 350002, China

[3]University of Chinese Academy of Sciences, Beijing 100049, China

Abstract: Graphene is regarded as a prominent multi-functional flame retardant for the use in halogen-free flame retardant polymer simultaneously with improved integrated properties and special functionalities. However, its flame retardant efficiency is not impressive enough due to the weak resistance to thermo-oxidative decomposition. In order to overcome this problem, the surface of graphene oxide was covered with large amounts of non-flammable silicas through a sol–gel and surface treatment process, and then used to modify the epoxy (EP) resin. Results show the incorporation of as-prepared nanosilica/graphene oxide (m-SGO) hybrid to EP resin not only obviously increases the flame retardancy, mechanical, and thermal stability properties, but also endows EP resin with high thermal conductivity, low dielectric loss, and high dielectric constant. Specifically, the peak of heat release rate and total

† Electronic supplementary information (ESI) available: The chemical structure of SGO and typical data from TG curves of EP and its nanocomposites (PDF).

* Corresponding author. Tel: +86 591 63173492. Fax: +86 591 63173494. E-mail: lxwu@fjirsm.ac.cn (Lixin Wu)

heat release of modified EP resin with 1.5 wt.% m-SGO are only 39 and 10 % of that of neat EP resin, respectively. These attractive features of m-SGO/EP nanocomposites are attributed to the unique structure and high resistance to oxidative degradation of m-SGO as well as their good interactions with EP resin. The investigation provides a new approach to preparing novel core-shell flame retardants through surface wrapping with other flame retardants on the SGO and related high performance flame retardant resins.

Keywords: epoxy resin; flame retardancy; nanocomposites; hybridized nanofiller

1. Introduction

Since the commercialization of the first synthetic resin in the early 20th century, thermosetting resins, acting as insulating paints, adhesives, matrices of composites, etc., have become important raw materials in many fields [1-4]. However, fire hazards associated with the use of these polymeric materials, which cause the loss of life and property, are of particular concern among government regulatory bodies, consumers, and manufacturers alike [5-7].

Heretofore, halogen-free flame retardants with outstanding flame retardancy simultaneously meeting the growing awareness of environmental protect are being pursued [8-10]; however, the addition of these developed flame retardants usually results in significant decrease of other original properties. Specifically, thermosets modified by the phosphorus-containing compounds usually exhibit decreased thermal stability, moisture resistance and toughness [11-13]; while for the inorganic flame retardants, 20%-60% loadings are usually necessary to meet the requirement of flame retardancy in applications. However such high levels of additives will in turn lead to significant deterioration of strength, toughness, processing characteristics, and dielectric properties [14]. It is still a challenge and an interesting subject to develop new halogen-free flame retardants which can not only significantly improve the flame retardancy, but also endow modified resins with other improved properties and special functionalities.

Recently, the use of nano-scaled fillers such as clays and carbon nanotubes (CNTs) to modify thermosets has attracted great interests from both industrial and academic researches [15-17]. It was found that these nanofillers can significantly improve the flame retardancy of thermosetting resins, while the mechanical properties, thermal stability, and moisture resistance are also simultaneously improved, making them become the promising halogen-free flame retardants [18, 19].

However, there are still some obstacles for the use of nano-scaled fillers as flame retardants. As for clays, their flame retarding efficiency has not been fully exerted because completely exfoliated clay/thermosets nanocomposites are hard to achieve [20, 21]. Moreover, neat clays cannot endow thermosetting resin with some special functionalities, such as electrostatic prevention, high thermal conductivity owing to their intrinsic physical nature. With regard to CNTs, their flame retardant efficiency is closely related to the formation of network structure. Since strong π–π stacking and Van der Waals force make CNTs to form bundles or aggregates, the surface treatment of CNTs is usually necessary to help the dispersion of CNTs in the matrix. However, the surface treatment usually causes serious damage on the graphitized-structure and aspect ratio of CNTs, and thus weakens the physical barrier effect of CNTs, leading to a loss of flame retardant efficiency and increasing cost [22]. In addition, it is known the barrier effect is the one of flame retardant mechanisms for nanomaterials, however, the linear structure of CNTs forms less barrier compared to those layered nanomaterials[23].

Graphene is a single layered carbon sheet, with high thermal conductivity, superior mechanical strength, and excellent electronic conductivity [24-27]. Compared with clays or CNTs, graphene shows the better potential for fabricating a high performance flame retarding material because it combines the advantages of both layered-structure and graphitized-structure. Heretofore, many efforts have been dedicated to employ graphene as a flame retardant in thermosetting resin [28, 29]. However, the bare graphene is prone to decompose under the combustion due to its weak thermal-oxidative stability, and thus reduces the physical barrier effect, ultimately resulting in a higher loading of graphene required to achieve an attractive flame retardancy [30].

In order to increase the flame retardancy efficiency of graphene, many researches have taken the oxygen-containing functionalities on the basal plane and along the edges as a platform to graft/cover other halogen-free flame retardants, such as intumescent flame retardant [31, 32], phosphorus-containing compounds [33, 34], layered double hydroxide (LDH) [35], metal oxide(sulfide) [36, 37], and polyhedral oligomeric silsesquioxanes (POSS) [38]. Notwithstanding the above research has proven that graphene with increased flame retardant efficiency can be achieved by surface modification, the flame retarding effect still can be further enhanced because the essence of graphene under thermal-oxidative atmosphere are not changed.

In this work, epoxy resin (EP) was chosen as the matrix resin for modification because EP is widely used in many civil and cutting-edge fields which urgently require improved flame retardancy. In order to alleviate thermal-oxidative decomposition of layered structure under the combustion, a novel graphene-based hybrid (m-SGO) consisting of graphene and nanosilica was prepared through a sol–gel and surface treatment process. Interestingly, this sandwich-like structure can transform into silica nanosheet under the process of combustion[39], and thus not only may inherit high flame retarding efficiency of inorganic layered clays, but also may endow resultant nanocomposites with special functionalities and outstanding mechanical properties. Accordingly, a series of modified EP resins using m-SGO were prepared, and the effects of m-SGO on the chemical structure, mechanical properties, dielectric properties, thermal stability, and flame retardancy of modified resin were investigated, and then a flame-retarding mechanism was proposed based on thorough evaluation and discussion. This investigation may lead to a new and efficient method to achieve combination of excellent flame retardancy and other improved properties in thermosetting resins.

2. Experimental

2.1. Materials

Nanosilica (15±5nm) was obtained from Shanghai Maikun Chemical Co. Ltd (China). Diglycidyl ether of bisphenol A (DGEBA) was purchased from Shanghai

Resin Factory Co. Ltd (China). The curing agent diethyltoluenediamine (DETDA) was obtained from the Chongshun Chemical Co. Ltd (China). Graphite was supplied by Aladdin Industrial Co. Ltd (China). H_2SO_4 (98 %), $NaNO_3$, $KMnO_4$, H_2O_2 (30 %), ethanol, ammonia (25–28 %), tetraethylorthosilicate (TEOS), and 3-triethoxysilylpropylamine were commercial product with analytical grades, and used without further purification. Distilled water was produced in our lab.

2.2. Preparation of graphene oxide

Graphene oxide was prepared using a modified Hummer's method from graphite powders [40, 41]. Typically, 3 g graphite, 1.5 g $NaNO_3$, and 144 mL of 98 wt.% H_2SO_4 were added to a three-necked bottle in an ice bath with vigorous stirring. Subsequently, 9 g $KMnO_4$ was slowly added, and the mixture was reacted at 15 ^oC for 1h and 50 ^oC for 30 min; then 144 mL distilled water was slowly added to the mixture which was below 70 ^oC. Afterward, temperature raised to 98 ^oC and maintained for 15 min, and then the mixture was poured into 600 ml of 10 wt.% H_2O_2 solution. Finally, a yellow powder was obtained after repeatedly washing with distilled water and completely drying at 50℃ in a vacuum oven, and named as GO.

2.3. Preparation and surface treatment of GO/nanosilica hybrid

50 mg GO was dispersed in 1200 mL of ethanol-water (5:1, v/v) solution by sonication for 30 min. After that, the pH of the reaction mixture was adjusted to 9.0 with ammonia solution, and then 0.5 mL of TEOS was added and the resulting solution stood for 24 h containing vigorous ultrasonic for more than 8h at room temperature. Subsequently, the suspension of product was centrifuged and washed 5

times with ethanol, and named as SGO.

Appropriate quantities of as-prepared SGO, 3-triethoxysilylpropylamine, distilled water, and ethanol were add with magnetic stirring for 4 h at 50 ^{o}C. Finally, a black powder was obtained after repeatedly washing with ethanol and completely drying at 50 ^{o}C in a vacuum oven, and named as m-SGO. The preparing process of m-SGO is shown in Scheme 1.

2.4. Preparation of EP resin and nanocomposites

Appropriate amounts of DGEBA and DETDA with a weight ratio of 1:0.234 were blended at 100 ^{o}C for 15 min with vigorous stirring to obtain a light yellow liquid, which was EP prepolymer. And then the mixture was thoroughly degassed in a vacuum oven at 110 ^{o}C for 30min, followed by pouring it into a pre-heated (100 ^{o}C) 'U'-type mold. Subsequently, the mold was put into an oven for curing and postcuring following the protocol of 120 ^{o}C/1 h + 180 ^{o}C/2.5 h and 190 ^{o}C/2 h, respectively, the resultant resin is a cured EP resin.

Appropriate amounts of GO, n-SiO_2, and m-SGO were respectively added into the mixture of EP prepolymer and ethanol by sonication for 30 min to form a black suspension, and then the mixture was degassed to remove excess solvent at 60 ^{o}C in a vacuum oven. After that the mixture was cast into a mold for curing and postcuring via the procedures of 120 ^{o}C/1 h + 180 ^{o}C/2.5 h and 190 ^{o}C/2 h, respectively. Finally, the resultant nanocomposites were demolded and coded as GO1.0/EP, $SiO_2$1.0/EP, and m-SGOn/EP, respectively, where 1.0 and n represent the weigh percent of used nanomaterial in the resultant nanocomposites (n=0.5, 1.0, and 1.5).

2.5. Characterization

Fourier Transform Infrared (FTIR) spectra were recorded using a PerkinElemer Spectrum One spectrometer (USA) from 400 to 4000 cm-1 with a resolution of 2 cm-1 (KBr pellet technique).

Raman Microscope (Renishaw, Invia, 514 nm) is used to determine the Raman scattering characteristics of the samples. The laser power used is 1 mW.

Atomic Force Microscope (AFM) measurements were performed to characterize the thickness and dimensions of as-prepared nanosheet using the Scanning Probe Microscopy (Veeco Instruments, Nanoscope Multimode IIIa, USA) operated in contact mode.

Transmission Electron Microscopy (TEM) was recorded on a JEM-2010 (JEOL, Japan) at a 200 kV accelerating voltage. The samples were prepared by mounting a drop of the micelle solution (0.05 mL) on a copper EM grid covered with a thin film of formvar.

A Scanning Electron Microscope (SEM) (HITACHI, SU8010/EDX, Japan) coupled with an energy disperse X-ray spectrometer (EDS) was employed to observe the morphologies of samples. The resolution of the secondary electron image is 1.5 nm under 15 kV. All samples should be dried at 50 °C for 24 h before test.

Thermogravimetric (TG) analyses were performed on a TA Instruments STA449C (USA) in the range from 25-800 °C under a nitrogen atmosphere with a flow rate of 100 ml/min and a heating rate of 10 °C/min.

Dynamic Mechanical Analysis (DMA) was performed using TA DMA Q800 apparatus from TA Instruments (USA). A single cantilever clamping mode was used. DMA tests were carried out from 25 °C to 200 °C with a heating rate of 3 °C/min at 1 Hz. The sample dimension was (35±0.02) × (13±0.02) × (3±0.02) mm^3.

The tensile property was performed according to ASTM D638 with a constant speed of 5 mm/min using a load cell of 1 kN. The results were averaged from five specimens.

Thermal conductivity at 20 °C was measured on a DRL-II thermal conductivity tester (Xiangtan Instrument and Meter Factory, China) using a steady-state method, and the upper copper plate was heated to 50 °C. The dimensions of each sample were Φ (30±0.02) mm × (3±0.02) mm. Three specimens were tested for each formulation, and the data reported herein are the averages of triplicate measurements.

The dielectric properties were measured by a Broadband Dielectric Spectrometer (Novocontrol Concept 80, Germany) in the frequency range 10–10^5 Hz at room temperature. The dimensions of the sample were (25±0.02) × (25± 0.02) × (3±0.02) mm^3.

LOI values were measured on a Stanton Redcraft Flame Meter (China) according to ASTM D2863/77. The dimensions of sample were (100±0.02) × (6.5±0.02) × (3±0.02) mm^3.

Flammability of the resins was characterized using a cone calorimeter performed in an FTT device (UK) according to ISO 5660 with an incident flux of 35 kW/m^2 using a cone shape heater. Typical results from cone calorimeter reported here were the averages of triplicate. The dimensions of the sample were (100 ± 0.02) × (100 ±

0.02) × (3 ± 0.02) mm^3.

3. Results and discussion

3.1. Characterization of GO and SGO

It is well known that GOs can be readily well-dispersed in water under suitable ultrasonic treatment, exhibiting a color of light yellow (Scheme 1); while their dispersibility in most of organic solvents is not good. Nevertheless, in order to obtain well-dispersed and exfoliated graphenes in polymer, organic solvents are generally needed as solvents in the dispersion of GO.. Heretofore, many investigations have been dedicated to improve the dispersion of GO in organic solvent [27].

Interestingly, it is noteworthy that the presence of nanosilicas has a significant influence on the solubility of GO in organic solvents. After the sol-gel and reduction processes, as-prepared SGO becomes hydrophobic, and thus readily form a stable colloidal suspension in ethanol (Scheme 1) due to the strong interaction between SGO and ethanol. In addition, there is a color transformation from yellow GO in water to black SGO in ethanol (Scheme 1), indicating that the reduction of GO occurs.

Fig. 1S ((ESI†)) depicts the FTIR spectrums of GO and SGO. It can be seen that four new absorption peaks at 1080, 950, 800, and 455 cm^{-1} appear in the spectrum of SGO, which are attributed to the asymmetric vibration and bending vibration of Si–O–Si and Si–OH and stretching vibration of Si–OH [42, 43], reflecting that the existence of silica in the SGO. Furthermore, after the process of sol–gel, the peak at 1080 cm^{-1} attributed to the asymmetric stretching vibration of C–O–Si appears, while the typical carbonyl group peak at 1728 cm^{-1} becomes very weak, suggesting that the interactions between as-produced silica and GO is covalent bonds. Altogether, these results preliminarily prove that large amounts of silica are successfully covered on the surface of GO by covalent bonds.

In order to obtain the detailed morphological transition of GO after reacting with TEOS and water, AFM and TEM observations were conducted as shown in Fig. 1. Fig. 1a-c show the AFM images of GO and SGO. It can be found that the size of most GO sheets is 0.2-1 μm and the thickness is ca. 1.0 nm（Fig. 1a）, indicating a complete exfoliation of graphite oxide into a single layer [44, 45]. After the process of sol-gel, large amounts of spherical nanosilica uniformly cover on the surface of GO as shown in Fig. 2b and 2c. In addition, the cross-section views illustrate that the average height of SGO and covered spherical nanosilica is ca. 9.0 nm and ca. 4.0 nm, respectively, and the surface of SGO is “puffy” due to the existence of spherical nanosilica.

The formation of “puffy” structure on the surface of SGO can be further confirmed by TEM images as shown in Fig. 1d-f. Pristine GO nanosheet exhibits a typically smooth layered structure, while SGO nanosheet shows a rough surface. Furthermore, as shown from Si mapping results of SGO, bright dots corresponding to Si atoms homogeneously distribute in the picture, reflecting that dense nanosilica uniformly cover on both sides of GO sheets without any obvious vacancies. As for the preparation of a graphene-based nanocomposite, it is intractable that pristine GO and graphene with fairly smooth surface are easy to re-stack to form bulky agglomerates in the drying process, which are difficult to re-exfoliate into single layered materials in the preparation of resultant nanocomposites. More interestingly, novel hybrid developed in this paper has a "puffy" structure due to the existence of substantial nanosilica on the surface of SGO, and then the introduced nanosilica can act as protuberances or spacers to prevent the re-stacking of SGO nanosheets. In view of such special structure, as-prepared SGO nanoparticles can be readily redispersed in solvents such as acetone and ethanol just under mild ultrasonic treatment, and thus contribute to obtaining a completely exfoliated graphene-based nanocomposite. Moreover, this rough "puff" structure can simultaneously endow the resultant nanocomposites with a good physical interaction between SGO and polymer matrix. Apparently, considering the characteristic resulting from the unique structure, it can be expect that nanocomposites based on as-prepared SGO will possess outstanding integrated properties.

Fig. 2 shows the XPS spectras of the GO and SGO. In the wide spectra (Fig. 2a), both spectras show sharp peaks at 286.7 and 532.6 eV, corresponding to C and O elements, respectively. The difference between the two spectras is that the spectrum of SGO has two additional Si_{2s} and Si_{2p} peaks at 153.9 and 103.8 eV, respectively, which is originated from the nanosilica. In order to further study the formation of chemical bonds between graphite layer and the introduced nanosilica, the narrow Si_{2p} spectrum of the SGO was also scanned. As shown in Fig. 2b, the Si_{2p} spectrum of SGO is fitted to three peaks at ca. 103.4, 103.1, and 102.6 eV, assigned to the Si–O–C, an 'inorganic SiO_2-like phase'[46], and Si–O–Ph[47], respectively, demonstrating that GO has been successfully covalent functionalized by nanosilica.

Raman scattering is strongly sensitive to the electronic structure and is proven to be an essential tool to characterize graphite and graphene materials [48]. As shown in Fig. 2S (ESI†), pristine GO demonstrates a strong band at 1601 cm^{-1} (G band) and a weak band at 1332 cm^{-1} (D band). The G and D bands are attributed to the sp^2 ordered crystalline graphite-like structures and a disordered sp^3 carbon structure, respectively. Compared with the GO, the peak position of as-prepared SGO does not shift. However, with careful observation, it can be seen that the relative intensity of the D and G bands undergoes a significant transformation, suggesting that an increase in ordered crystalline graphite-like structures within as-prepared SGO. Since the noncovalent bonding between carbon structure and silica tends to show no significant variation of band shift or relative intensity after the coating process [49], it can be concluded that the nanosilica are deposited on the surfaces of GO by covalent bonds, which ultimately leads to the reduction of GO.

Based on above analysis, a partially reduced nanosilica-hybridized GO with good dispersion on organic solvents is successfully prepared by chemically bonding large amounts of nanosilica on the surface of GO.

3.2. The structure of cured EP nanocomposites

Macro-performance of a material is determined by its structure. For a nanocomposite, its structure is divided into macro-structure and micro-structure. Specifically, the former can be reflected by the dispersion of nanofillers, and the latter can be characterized by the interfacial interactions, curing mechanism, and cross-linking density of matrix.

As for the EP system used in this paper, its main curing reaction is the ring opening addition reaction between the amino group and epoxide group [50]. In order to increase the interfacial interactions between the SGO and EP resin, functional groups which can form chemical bonding with epoxide group were introduced on the surface of SGO. Herein, the $-NH_2$ group was designed to be introduced on the surface of as-prepared new hybrid (m-SGO) through the surface treatment of SGO with 3-triethoxysilylpropylamine as shown in Scheme 1, toward combination of good flame retardancy and other properties.

In general, graphite oxide is hard to completely exfoliate into single layer GOs due to its hydrophilic and poor dispersion on organic solvent, and then some GOs still exist in the form of multi-layer stacks [51]. Moreover, pristine GO is hard to react with epoxide group without catalyst, and thus a weak interfacial interaction exists between GO and EP resin. Compared with GO1.0/EP nanocomposites, the improved interfacial interaction and dispersion of m-SGO1.5/EP can be observed by SEM images of their fractured surfaces, as shown in Fig. 3. It can be seen that both GO and m-SGO are well dispersed in the EP matrix without any significant aggregation in low magnification but exhibit an extraordinary difference in the interfacial interaction between the matrix and nanofillers. Specifically, the GOs are partly protruded out from the fracture surface of GO1.0/EP nanocomposite, exhibiting a weak interfacial interaction, while no pulled or agglomerate m-SGO exists in the picture, indicating a good dispersion of m-SGO in EP matrix and strong interfacial interactions.

It is known that the modulus of the rubber plateau for polymer networks are generally related to the cross-linking density of the materials [52, 53]. Fig. 4 shows the overlay storage moduli (E') as a function of temperature for EP resin and resultant nanocomposites, it is noted that the cross-linking densities of m-SGO/EP are larger than that of EP resin, $SiO_2$1.0/EP, and GO1.0/EP, and the m-SGO/EP nanocomposites with the larger content of m-SGO have a higher E'. Generally, the cross-linking density means the concentration of cross-linked bonds per volume. As for a typical polymer nanocomposite, the presence of nanomaterial usually results in the loose stacking of the macromolecules surrounding the solid particles and forming additional organic network[54, 55], and then decreases the cross-linking density of $SiO_2$1.0/EP and GO1.0/EP nanocomposites. However, compared with the structure of GO and SiO_2, that of m-SGO contains a lot of $-NH_2$ groups meaning that the presence of m-SGO tends to shorten the distance among cross-linking points, and thus increases the cross-linking density of the resultant network.

Based on the above discussion, it can be stated that the addition of m-SGO to EP resin significantly changes the structure of the resultant network. Such changes in network structure will in turn affect the macroscopic properties of the EP resin.

3.3. Typical properties of cured m-SGOn/EP nanocomposites

As described above, the aim of this work is to develop new flame retarding resin with significantly improved integrated performance and special functionality, hence before the discussion of flame retardancy, it is necessary to evaluate other typical properties of m-SGO/EP nanocomposites.

Table 1 shows the glass transition temperature (T_g), tensile strength, and thermal conductivity of cured EP resin and resultant nanocomposites. It is attractive to find out that all m-SGO/EP nanocomposites have higher values of T_g, tensile strength, and thermal conductivity than those of EP resin, and the more content of m-SGO is introduced into nanocomposites, the bigger improvement in these properties is shown. Specifically, the T_g value of the m-SGO1.5/EP nanocomposite shifts toward higher temperature by ca.10 ^{o}C, and the tensile strength and thermal conductivity of m-SGO1.5/EP nanocomposite are ca. 1.31 and 1.38 times of that of EP resin, respectively; meanwhile, these properties of m-SGO1.0/EP nanocomposite are better than that of $SiO_2$1.0/EP or GO1.0/EP nanocomposite, indicating that the covalent combination of GO and SiO_2 exhibits a synergistic effects on the properties of resultant nanocomposites. These attractive improvements in integrated properties for m-SGO/EP nanocomposites are attributed to the change in structure of polymeric network, the excellent mechanical strength and special rough surface as well as superhigh thermal conductivity of SGO, good dispersion of m-SGO on the matrix, and strong interfacial interactions between m-SGO and resin matrix.

The dielectric constant and loss of cured EP and resultant nanocomposites as a function of frequency are shown in Fig. 5. It can be seen that (1) all m-SGO/EP nanocomposites exhibit very good stability of dielectric constant over a wide frequency range from 10 to 10^6 Hz as neat EP resins does; moreover, the dielectric constant of m-SGO1.0/EP nanocomposite is obviously higher than that of nanocomposites with the same content of GO or SiO_2. As it is known that the dielectric constant of a material is a function of its capacitance, which is proportional to the quantity of the charge stored on either surface of the material in an applied electric field. With m-SGO/EP nanocomposites, the good dispersion of m-SGO in the matrix and high electrical conductivity of m-SGO cause the formation of more efficient charge stored place than that of GO/EP or SiO_2/EP, resulting in a bigger dielectric constant. (2) It is interesting to find that compared with GO/EP nanocomposite, all m-SGO/EP nanocomposites have lower dielectric loss at low frequency (＜10^3 Hz). It is known that the dielectric loss when the frequency is lower than 10^3Hz results from the Maxwell–Wagner effect (the space charge or interfacial polarization mechanism). As for a nanocomposite, there is the interfacial polarization because of the accumulation of charges at the interfaces. Compared with m-SGO/EP nanocomposites, the GO in GO/EP nanocomposite is hard to achieve good dispersion as describe above, and thus leading to a high dielectric loss at low frequency (＜10^3 Hz). This is attractive in some electric and power industries, when they are developing and looking for novel materials with high dielectric constant and low dielectric loss.

Fig. 6 shows the TG curves of GO, SGO, EP, and all nanocomposites in a nitrogen atmosphere, and the corresponding initial degradation temperature (T_{di}) at which the weight loss of the sample reaches 5 wt.%, the maximum degradation rate temperature (T_{max}), and char yield (Y_c) at 750 ^oC are summarized in Table 1S (ESI†). It can be seen that all m-SGO/EP nanocomposites have similar values of T_{di} and T_{max} as EP resin does, indicating that they have similar thermal degradation mechanism. Furthermore, it is worthy to note that the Y_c values of m-SGO1.0/EP nanocomposites are significantly higher than that of GO1.0/EP or $SiO_2$1.0/EP nanocomposites as well as theoretical values calculated by the "Mixture Rule". The reasons behind this phenomenon can be explained by the effect of SGO on the crosslinking structure as well as the characteristic of SGO under thermal degradation. On the one hand, as described above, the introduced SGO can increase the crosslinking density of EP network, and then play a positive role on improving the thermal stability. On the other hand, during the process of degradation, the SGO can transform into the silica nanosheets possessing excellent thermal-oxidative degradation resistance[39], which can also be confirmed by the morphology and elemental composition of m-SGO after calcining at 700 ^{o}C by SEM and EDS analyses as shown in Fig. 7. In accordant with the previous report[38], the m-SGO can be transformed into silica nanosheets under the high temperature thermo-oxidative degradation, and then create a "Tortuous path" to form a gas barrier [56], which can not only delays the thermal decomposition of organic resin, but also reduce the volatilizing rate of decomposition products. Above two influences combine together, and thus lead to the non-proportionally increased residual char of nanocomposites.

In conclusion, it is interesting to note that the addition of m-SGO to EP resin can not only significantly improve thermal stability and mechanical properties of EP resin, but also endow it with special functionalities, such as high dielectric constant and low dielectric loss, increased thermal conductivity, etc..

3.4. Flame retardancy and mechanism of cured m-SGOn/EP nanocomposites

3.4.1 Flame retardancy

There are several methods to predict the combustion behavior of a material in real fires, of them LOI and cone calorimetry are two important ones. The former quantitatively determines the ability to ignite, while the latter gives useful information about the burning behavior [57].

Fig. 8 shows the LOI values of cured EP resin and its nanocomposites. It can be seen that the LOI value of epoxy resin increases with the addition of m-SGO. Specifically, the cured m-SGO1.0/EP composite has the maximum LOI value, which is about 1.11 times of that of neat EP resin and also much higher than that of $SiO_2$1.0/EP nanocomposite and that of GO1.0/EP nanocomposite, indicating the synergistic flame retardant effect of GO and SiO_2.

Fig. 9 shows the curves from cone calorimeter analyses for cured EP and its nanocomposites, and the typical data are also summarized in Table 2. Heat release rate (HRR), including peak heat release rate (PHRR) and total heat release (THR), and time to PHRR are three important parameter representing the degree of difficulty in igniting a material. It can be seen that the incorporation of m-SGO to EP resin can significantly slow down the combustion process. Specifically, compared with EP resin, the m-SGO1.5/EP nanocomposites displays 39 and 10 % reduction in the PHRR and THR, respectively, while its value of time to PHRR also lengthens 4 s. In addition, compared with $SiO_2$1.0/EP or GO1.0/EP nanocomposites, it is noticeable that m-SGO1.0/EP nanocomposite also has a better flame retardancy, further demonstrating that a remarkable synergetic effect between the GO and SiO_2 on the enhanced flame retardancy can be exerted through covalent functionalizing of nanosilica on the surface of GO.

Compared with the traditional layered nanomaterials, such as graphene, organclay, layered double hydroxides, etc., the novel m-SGO hybrid developed herein i) under the process of combustion: it can transform into silica nanosheets which possess high thermo-oxidative stability and radius-thickness ratio, and thus may exert high flame retarding efficiency of layered structure; ii) under the service temperature: it can endow modified resin with special functionality and outstanding mechanical properties due to its graphene-based framework and rough surface nature. Herein, as expected, the m-SGO successfully endows modified EP resin with improved flame retardancy, mechanical, and thermal stability properties as well as additional dielectrics and thermal conductivity properties, which meets the necessary requirements for the fabrication of a novel high performance flame retardancy material. Not only that, this hybrid developed in this paper can also be made as a template to introduce other flame retardants with special flame retarding effects as described in the Introduction part, and then exhibits a higher flame retardancy efficiency compared with that of m-SGO.

3.4.2 Flame retarding mechanism

It is known that the flame retardancy of a polymer usually depends on several factors, among which the crosslinking density is the key one [58, 59]. As describe above, the incorporation of m-SGO into EP resin is beneficial to increase the crosslinking density of the resultant nanocomposites, and thus plays a positive role in improving the flame retardancy of EP resin.

Besides the crosslinking density, the physical properties (yield, structure, mechanical properties, expansion ratio, etc.) and the chemical properties (thermal stability, thermal conductivity, etc.) of the residual char for a material are also dependent on the flame retardancy of the material [60]. Since the flame retarding mechanism of layered materials is thought to be the formation of a protective barrier during combustion [61], hence the obviously increased value of Y_c with the addition of m-SGO to EP resin as described above contributes to getting better flame retardancy compared with EP resin. In addition, the information on the morphology and composition of the residual char can be obtained from SEM technique coupled with EDS, which then allows for evaluating the influence of char on the flammability. Fig. 10 shows the SEM micrographs of the residual chars of EP and m-SGO1.5/EP composites after combustion tests. Compared with the residual char of EP resin, that of m-SGO1.0/EP nanocomposite presents a compact and porous char layer. More interestingly, EDS analysis (Table 3) shows that the weight percent of silicon in the exterior and interior of the residual char is 1.2 wt.% and 0.3 wt.% respectively. The combustion and degradation of polymers on the surface consume more carbon in the exterior layer than that in the interior, and thus increase the relative content of Si elements in the exterior, resulting in higher percent of silicon in the exterior. The high percentage of silicon in turn slows down the further loss of carbon by the barrier effect.

Based on the aforementioned discussions, it can be concluded that m-SGO can increase the crosslinking density of EP resin and effectively retard the thermal degradation during the whole degradation process due to its structural transformation under thermal treatment, and thus delay the thermal degradation of polymer chain segments, ultimately leading to a superior flame retarding effect. In other words, a condensed phase mechanism accounts for the improved flame retardancy of m-SGOn/EP nanocomposites. Fig. 11 represents the schematic flame retarding mechanisms of m-SGOn/EP systems. Briefly, when they are heated to a certain temperature, the epoxy matrix starts to degrade; meanwhile, under this condition, the m-SGO in the matrix transform to silica nanosheets with high resistance to oxidative degradation. Owing to their good dispersion in the EP matrix as well as strong interfacial interactions between m-SGO and EP matrix, the transformed silica nanosheets can play a key role in gas barrier effect, which not only significantly increases the char-forming ability, but also isolates the resin from oxygen and heat through a "Tortuous path" mode, so the m-SGOn/EP nanocomposites have high flame retardancy.

4. Conclusions

A graphene-based hybrid (m-SGO) consisting of graphene and nanosilica was prepared through sol–gel and surface treatment process, which can significantly improve flame retardancy and other typical properties of epoxy resin simultaneously. Specifically, the incorporation of m-SGO to epoxy resin can reduces the flammability (including PHRR, THR, and LOI, etc..). These attractive performances can be attributed to the unique structure and high resistance to oxidative degradation of m-SGO as well as their good interactions with EP resin. It is interesting to note that the m-SGO can not only be used as a multi-functional modifier to improve the thermal stability, mechanical, thermal conductivity, and dielectric properties due to their graphene-based framework, but also can act as an efficient flame retardant of EP resin because this novel layered hybrids can transform into silica nanosheets with high resistance to oxidative degradation under high temperature.

Acknowledgements

This research was financially the National Natural Science Foundation of China (Grant No.: U1205114 and 51403212), the Science Foundation of Fujian province (Grant No.: 2013H0062), and the "Strategic Priority Research Program" of the Chinese Academy of Sciences (Grant No.: XDA09020301).

Notes and references

1 D. Vennerberg, Z. Rueger and M. R. Kessler, *Polymer,* 2014, **55**, 1854.

2 J. Zhang, S. Deng, Y. Wang, L. Ye, L. Zhou and Z. Zhang, *Compos. Part. A*, 2013, **55**, 35.

3 S. G. Prolongo, G. del Rosario and A. Ureña, *Int. J. Adhes. Adhes.,* 2006, **26**, 125.

4 Z. Yan, W. Liu, H. Wang, K. Su and G. Xia-Hou, *J. Fluorine. Chem.,* 2014, **157**, 63.

5 P. T. Chung, C. T. Yang, S. H. Wang, C. W. Chen, A. S. T. Chiang and C.-Y. Liu, *Mater. Chem. Phys.,* 2012, **136**, 868.

6 L. Guadagno, M. Raimondo, V. Vittoria, L. Vertuccio, C. Naddeo, S. Russo, B. De Vivo, P. Lamberti, G. Spinelli and V. Tucci, *Rsc Adv,* 2014, **4**, 15474.

7 A. Toldy, B. Szolnoki and G. Marosi, *Polym. Degrad. Stab.,* 2011, **96**, 371.

8 Z. Matusinovic and C. A. Wilkie, *J. Mater. Chem.,* 2012, **22**, 18701.

9 B. K. Kandola and A. R. Horrocks, *Polym. Degrad. Stab.,* 1996, **54**, 289.

10 S. Jiang, Y. Shi, X. Qian, K. Zhou, H. Xu, S. Lo, Z. Gui and Y. Hu, *Ind. Eng. Chem. Res.,* 2013, **52**, 17442.

11 C. S. W. C.H. Lin, *Polymer*, 2001, **42**, 1869.

12 C. Xie, B. Zeng, H. Gao, Y. Xu, W. Luo, X. Liu and L. Dai, *Polym. Eng. Sci.*, 2014, **54**, 1192.

13 S. X. Cai and C. H. Lin, *J. Polym. Sci. Pol. Chem.,* 2005, **43**, 2862.

14 M. Zhang, P. Ding and B. Qu, *Polym. Compos.,* 2009, **30**, 1000.

15 B. Pradhan, S. K. Srivastava, R. Ananthakrishnan and A. Saxena, *J. Appl. Polym. Sci.,* 2011, **119**, 343.

16 X. Wang, W. Xing, P. Zhang, L. Song, H. Yang and Y. Hu, *Compos. Sci. Technol.,* 2012, **72**, 737.

17 F. Piscitelli, A. M. Scamardella, V. Romeo, M. Lavorgna, G. Barra and E. Amendola, *J. Appl. Polym. Sci.,* 2012, **124**, 616.

18 T. Kashiwagi, F. Du, J. F. Douglas, K. I. Winey, R. H. Harris, Jr. and J. R. Shields, *Nat. Mater.,* 2005, **4**, 928.

19 H. Ma, L. Tong, Z. Xu and Z. Fang, *Nanotechnology*, 2007, **18**, 375602.

20 J. M. Herrera-Alonso, E. Marand, J. C. Little and S. S. Cox, *J. Membrane. Sci.*, 2009, **337**, 208.

21 H. L. X. Kornmann, L.A. Berglund, *Polymer,* 2001, **42**, 1303.

22 S. Peeterbroeck, F. Laoutid, B. Swoboda, J.-M. Lopez-Cuesta, N. Moreau, J. B. Nagy, M. Alexandre and P. Dubois, *Macromol. Rapid. Comm.*, 2007, **28**, 260.

23 F. Laoutid, L. Bonnaud, M. Alexandre, J. M. Lopez-Cuesta and P. Dubois, *Mater. Sci. Eng. R-Rep.*, 2009, **63**, 100.

24 K. A, Geim. K, S, Novoselov, *Nat. Mater.,* 2007, **6**, 183.

25 C. N. Rao, A. K. Sood, K. S. Subrahmanyam and A. Govindaraj, *Angew. Chem.*, 2009, **48**, 7752.

26 R. Verdejo, M. M. Bernal, L. J. Romasanta and M. A. Lopez-Manchado, *J. Mater. Chem.,* 2011, **21**, 3301.

27 H. Yang, C. Shan, F. Li, Q. Zhang, D. Han and L. Niu, *J. Mater. Chem.,* 2009, **19**, 8856.

28 S. Liu, H. Yan, Z. Fang and H. Wang, *Compos. Sci. Technol.,* 2014, **90**, 40.

29 N. Hong, J. Zhan, X. Wang, A. A. Stec, T. Richard Hull, H. Ge, W. Xing, L. Song and Y. Hu, *Compos. Part. A*, 2014, **64**, 203.

30 P. Liu, Y. Huang and X. Zhang, *Compos. Sci. Technol.,* 2014, **95**, 107.

31 G. Huang, S. Chen, P. Song, P. Lu, C. Wu and H. Liang, *Appl. Clay. Sci.*, 2014, **88-89**, 78.

32 J. N. Gavgani, H. Adelnia and M. M. Gudarzi, *J. Mater. Sci.*, 2013, **49**, 243.

33 X. Qian, L. Song, B. Yu, B. Wang, B. Yuan, Y. Shi, Y. Hu and R. K. K. Yuen, *J. Mater. Chem. A.*, 2013, **1**, 6822.

34 C. Bao, Y. Guo, B. Yuan, Y. Hu and L. Song, *J. Mater. Chem.*, 2012, **22**, 23057.

35 X. Wang, S. Zhou, W. Xing, B. Yu, X. Feng, L. Song and Y. Hu, *J. Mater. Chem.* A, 2013, **1**, 4383.

36 C. Bao, L. Song, C. A. Wilkie, B. Yuan, Y. Guo, Y. Hu and X. Gong, *J. Mater. Chem.*, 2012, **22**, 16399.

37 S.-D. Jiang, Z.-M. Bai, G. Tang, Y. Hu and L. Song, *Ind. Eng. Chem. Res.,* 2014, **53**, 6708.

38 X. Wang, L. Song, H. Yang, W. Xing, B. Kandola and Y. Hu, *Ind. Eng. Chem. Res.*, 2012, **22**, 22037.

39 L. Kou and C. Gao, *Nanoscale*, 2011, **3**, 519.

40 W. S. O. Hummers, R. E, *J. Am. Chem. Soc.*, 1958, **80**, 1339.

41 R. C.-S. Laura J. Cote, and Jiaxing Huang, *J. Am. Chem. Soc*., 2009, **131**, 11027.

42 C. Chen, S. Shi, M. Wang, H. Ma, L. Zhou and J. Xu, *J. Mater. Chem.* A., 2014, **2**, 8126.

43 Y. Yang, S. Qiu, W. Cui, Q. Zhao, X. Cheng, R. K. Y. Li, X. Xie and Y.-W. Mai, *J. Mater. Sci.*, 2009, **44**, 4539.

44 C. Bao, Y. Guo, L. Song, Y. Kan, X. Qian and Y. Hu, *J. Mater. Chem.*, 2011, **21**, 13290.

45 J. Wu, G. Huang, H. Li, S. Wu, Y. Liu and J. Zheng, *Polymer*, 2013, **54**, 1930.

46 Y. Liu, Y. Shi, D. Zhang, J. Li and G. Huang, *Polymer*, 2013, **54**, 6140.

47 Z. Wang, P. Wei, Y. Qian and J. Liu, *Compos. Part B-Eng.*, 2014, **60**, 341.

48 J. Ma, Q. Meng, A. Michelmore, N. Kawashima, Z. Izzuddin, C. Bengtsson and H.-C. Kuan, *J. Mater. Chem.* A., 2013, **1**, 4255.

49 S. Chen, M. Levendorf, W. Cai, S.-Y. Ju, J. Edgeworth, X. Li, C. Magnuson, A. Velamakanni, Richard D. Piner, J. Kang, J. Park and R. S. Ruoff, *ACS Nano*, 2011, **5**, 1321.

50 S. Ganguli, A. K. Roy and D. P. Anderson, *Carbon*, 2008, **46**, 806.

51 Q. Liu, X. Zhou, X. Fan, C. Zhu, X. Yao and Z. Liu, *Polym.-Plast. Techn.*, 2012, **51**, 251.

52 W. K. Goertzen and M. R. Kessler, *Compos. Part. A*, 2008, **39**, 761.

53 H. C. Song., Beijing University of Aeronautics & Astronautics Press, Beijing, China, 1985, pp156-200.

54 M. Ree, J. Yoon and K. Heo, *J. Mater. Chem.*, 2006, **16**, 685.

55 Q. Li, S. L. Simon, *Macromolecules*, 2008, **41**, 1310.

56 C. L. J. Jeffrey W. Gilman, A. B. Morgan and R. Harris, *Chem. Mater.*, 2000, **12**, 1866.

57 D. Zhuo, A. Gu, G. Liang, J.-t. Hu, L. Yuan and X. Chen, *J. Mater. Chem.*, 2011, **21**, 6584.

58 L. Abate, I. Blanco, G. Cicala, A. Mamo, G. Recca and A. Scamporrino, *Polym. Degrad. Stab.,* 2010, **95**, 798.

59 Y. Han, J. Zhang, L. Shi, S. Qi, J. Cheng and R. Jin, *Polym. Degrad. Stab.,* 2008, **93**, 242.

60 H. Lu and C. A. Wilkie, *Polym. Degrad. Stab.,* 2010, **95**, 2388.

61 A. A. D. L. VanderHart, J. W. Gilman, *Macromolecules*, 2000, **34**, 3819.

Table 1 Typical properties of cured EP resin and its nanocomposites

Formulation	T_g (℃)	Tensile strength (MPa)	Coefficient of thermal conductivity (W/m.K)
EP	189	54 ± 3	0.21
$SiO_2$1.0/EP	188	56 ± 2	0.24
GO1.0/EP	177	66 ± 4	0.22
m-SGO0.5/EP	190	62 ± 3	0.25
m-SGO1.0/EP	196	68 ± 4	0.27
m-SGO1.5/EP	199	71 ± 5	0.29

Table 2 Selected cone calorimeter data for pure EP and its nanocomposites

samples	t_{ign} (s)	PHRR (kW/m^2)	PHRR reduction (%)	THR (MJ/m^2)	Time to PHRR(s)
EP	68	1471	-	108.67	152
$SiO_2$1.0/EP	67	1420	3.5	106.31	143
GO1.0/EP	65	1235	16.04	101.9	146
m-SGO0.5/EP	67	1279	13.05	102.95	145
m-SGO1.0/EP	66	1129	23.27	101.93	158
m-SGO1.5/EP	66	894	39.23	98.38	156

Table 3 Elemental compositions of the residual char of EP and m-SGO1.5/EP

Sample		Elemental composition (wt.%)		
		C	O	Si
Residue of EP	Exterior	82.8	17.2	-
	Interior	83.1	16.9	-
Residue of m-SGO1.5/EP	Exterior	80.3	18.5	1.2
	Interior	84.7	15.0	0.3

Captions of Scheme and Figures

Fig. 1 AFM, TEM, and Si maping (EDS) images of GO and SGO

Fig. 2 XPS spectra of GO and SGO (a), and the Si2p XPS spectrum of SGO (b)

Fig. 3 SEM images of cured EP and its nanocomposites

Fig. 4 Plots of storage modulus (E') as a function of temperature for cured EP and its nanocomposites

Fig. 5 Dependence of dielectric constant and loss on frequency of cured EP and its nanocomposites

Fig. 6 TG curves of GO, SGO, EP, $SiO_2$1.0/EP, GO1.0/EP, and m-SGO/EP in a nitrogen atmosphere

Fig. 7 SEM micrographs (A and B) and EDX (C) result of m-SGO after calcining at 700 ^oC

Fig. 8 LOI values of cured EP and its nanocomposites

Fig. 9 Dependence of heat release rate on time of pure EP and its nanocomposites

Fig. 10 SEM micrographs of residual chars for cured EP and m-SGO1.5/EP

Fig. 11 Schematic combustion processes of m-SGO/EP nanocomposites

Scheme 1 Schematic illustration for the preparation of modified nanolsilica/graphene hybrid

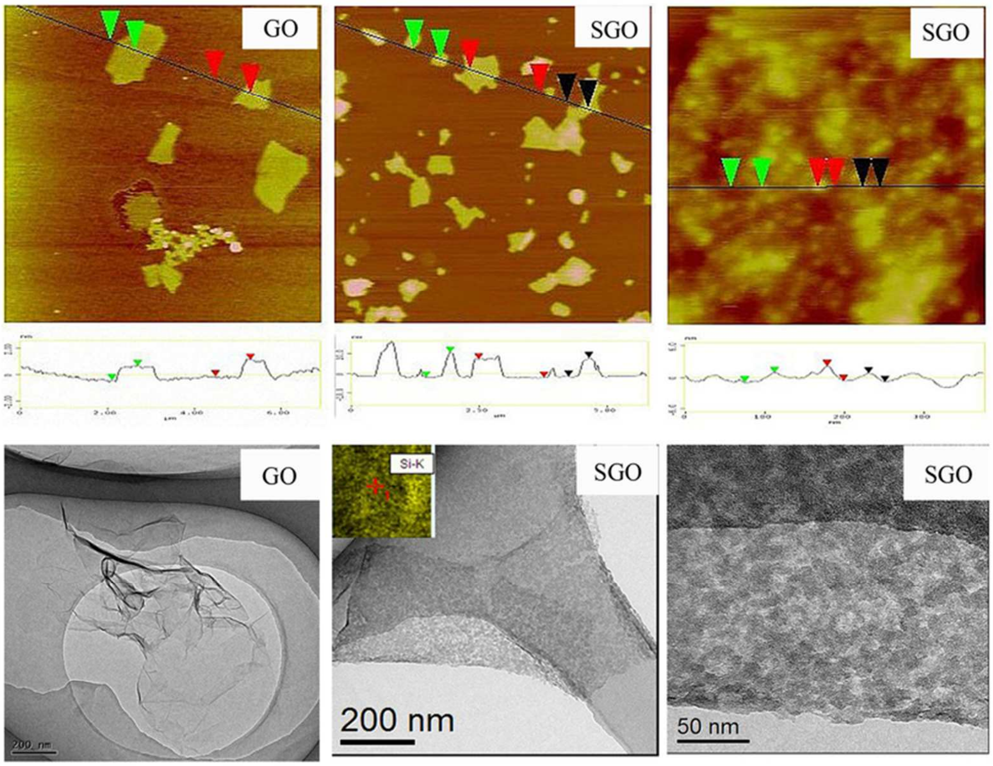

Fig.1 AFM, TEM, and Si maping (EDS) images of GO and SGO
69x53mm (300 x 300 DPI)

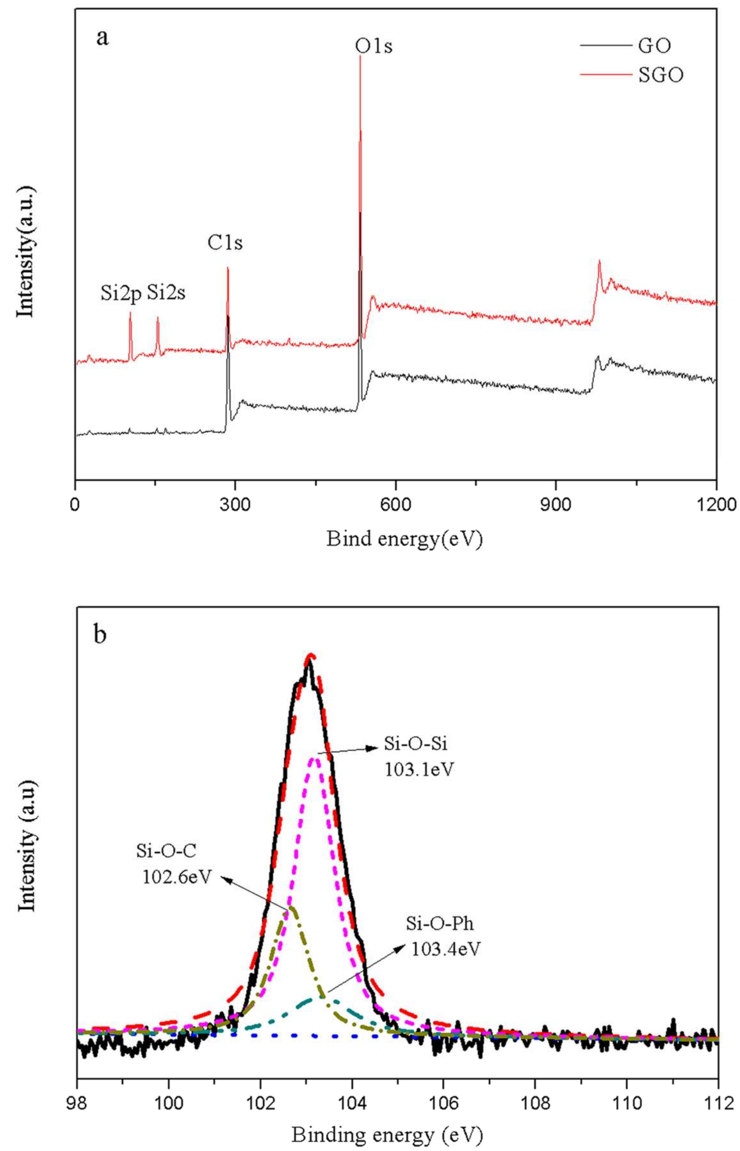

Fig.2 XPS spectra of GO and SGO (a), and the Si2p XPS spectrum of SGO (b)
127x181mm (300 x 300 DPI)

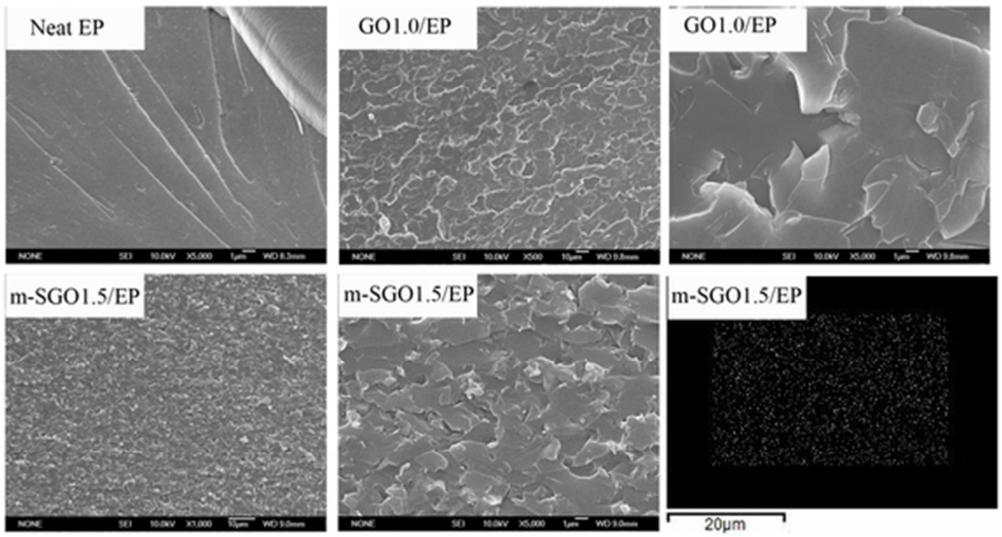

Fig. 3 SEM images of cured EP and its nanocomposites
48x26mm (300 x 300 DPI)

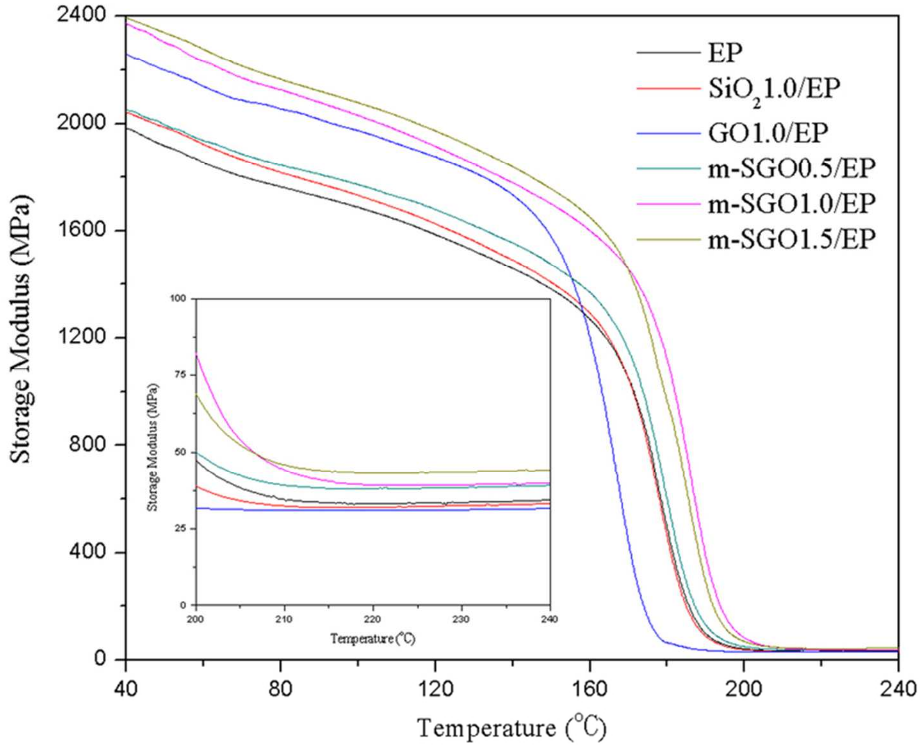

Fig.4 Plots of storage modulus (E’) as a function of temperature for cured EP and its nanocomposites
73x60mm (300 x 300 DPI)

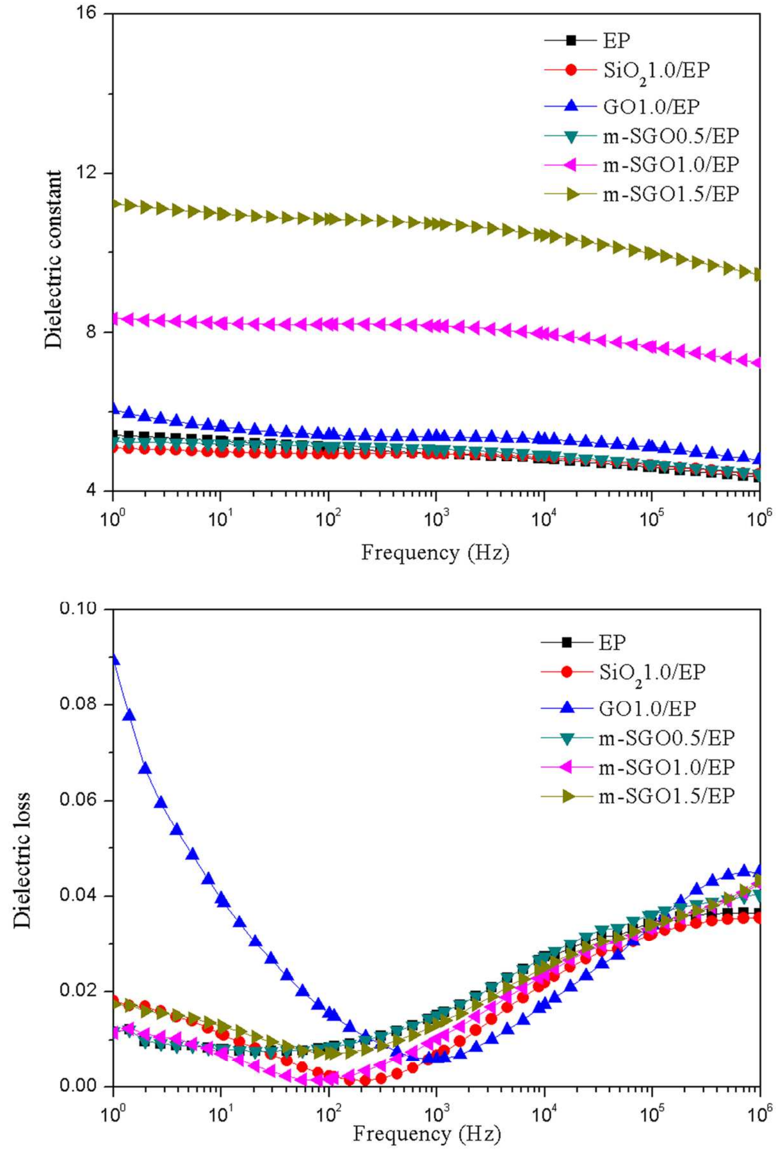

Fig.5 Dependence of dielectric constant and loss on frequency of cured EP and its nanocomposites
130x190mm (300 x 300 DPI)

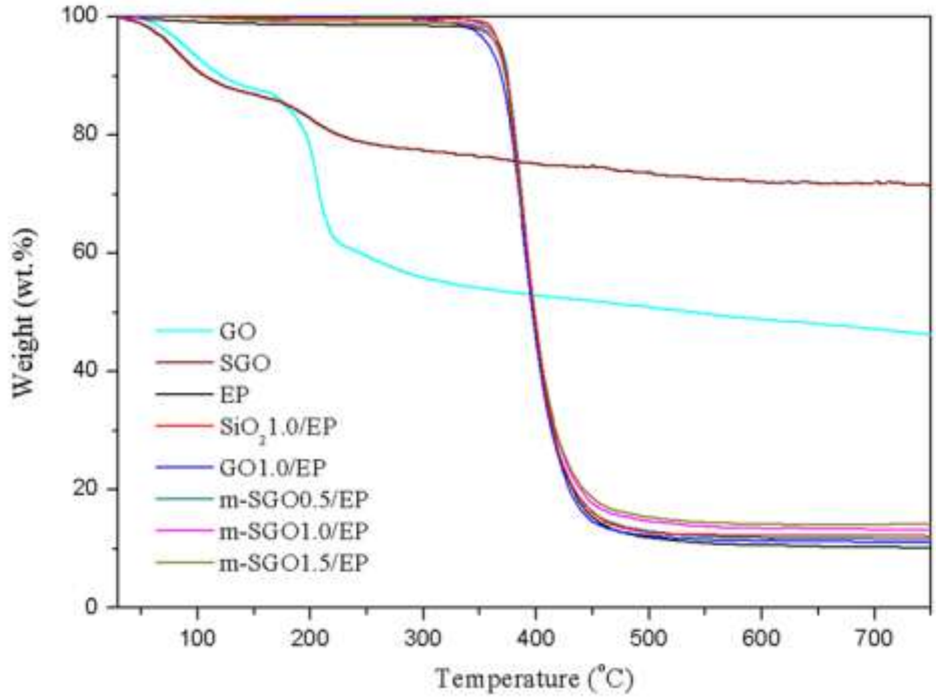

Fig.6 TG curves of GO, SGO, EP, SiO21.0/EP, GO1.0/EP, and m-SGO/EP in a nitrogen atmosphere
67x51mm (300 x 300 DPI)

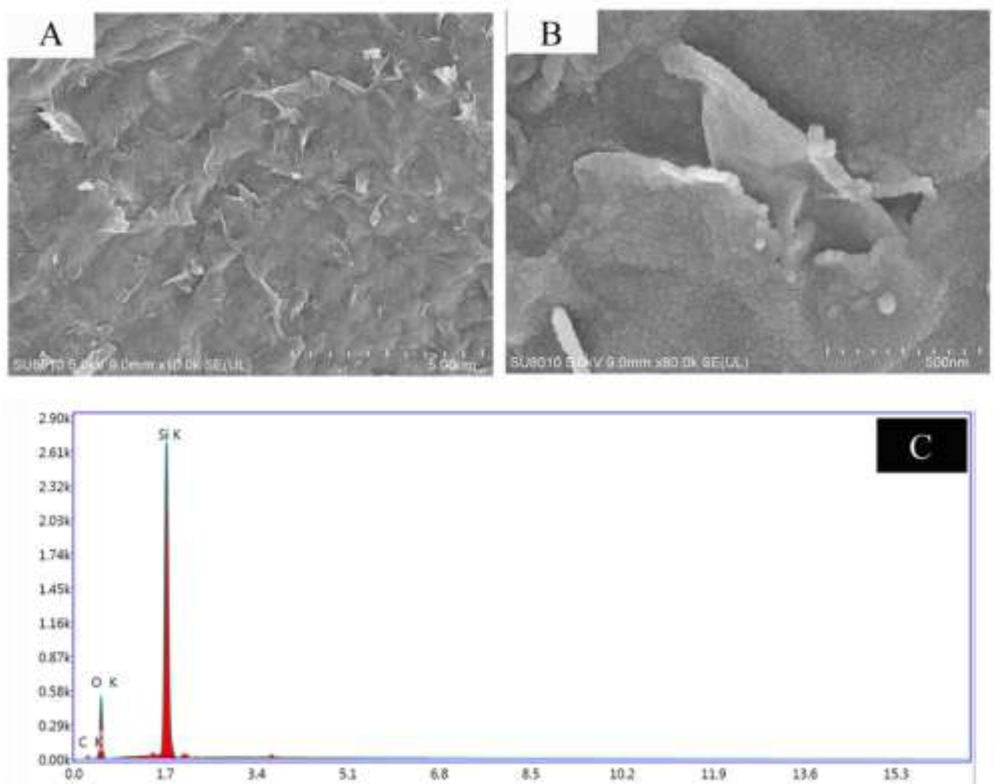

Fig.7 SEM micrographs (A and B) and EDX (C) result of m-SGO after calcining at 700 oC
73x61mm (300 x 300 DPI)

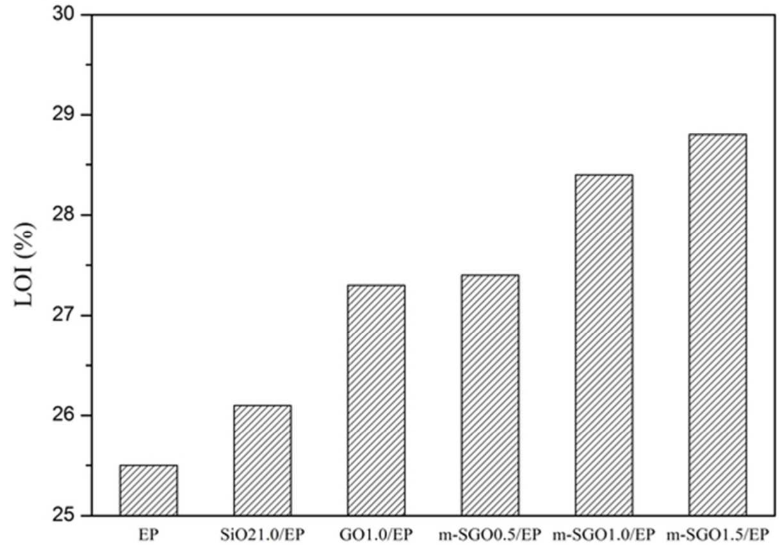

Fig. 8 LOI values of cured EP and its nanocomposites
62x43mm (300 x 300 DPI)

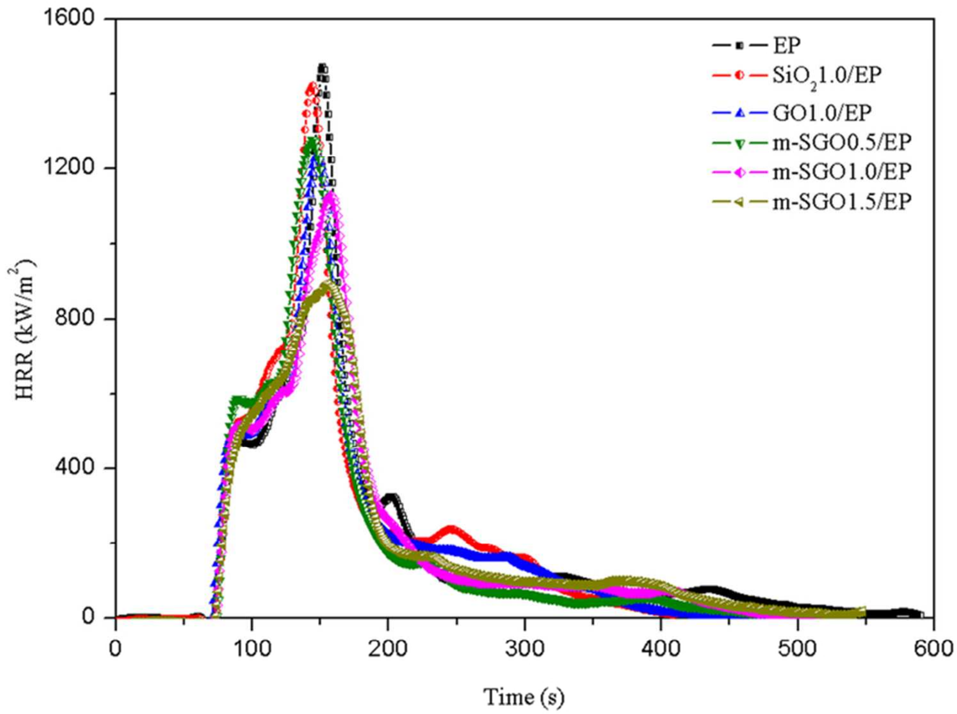

Fig.9 Dependence of heat release rate on time of pure EP and its nanocomposites
68x53mm (300 x 300 DPI)

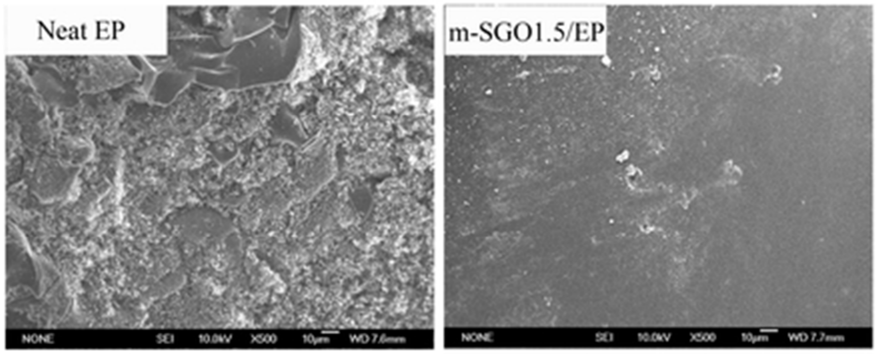

Fig.10 SEM micrographs of residual chars for cured EP and m-SGO1.5/EP
36x15mm (300 x 300 DPI)

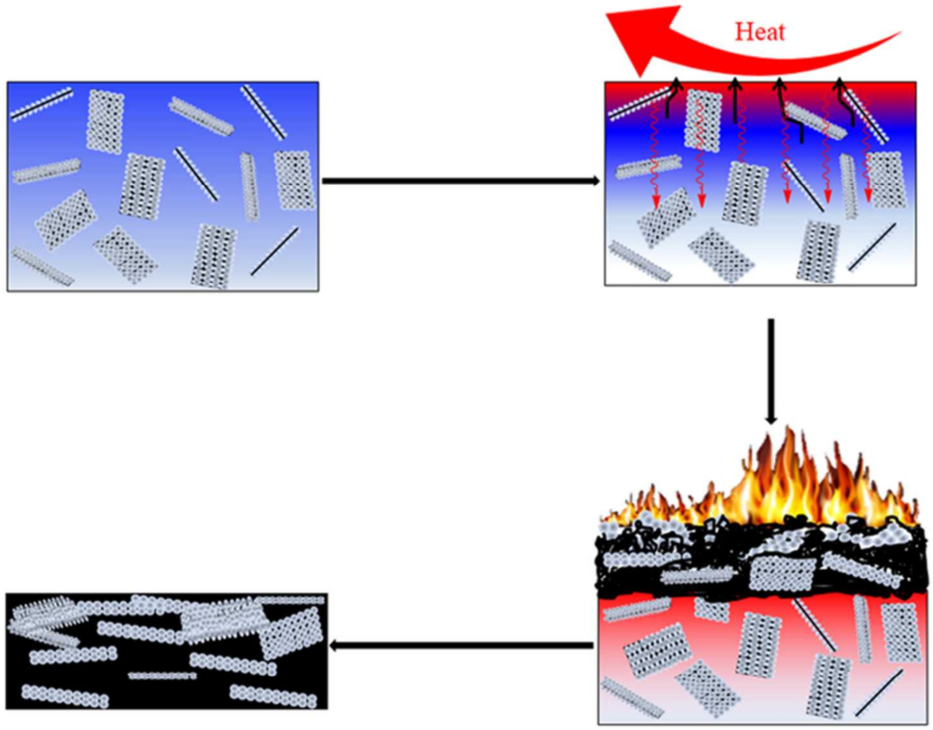

Fig.11 Schematic combustion processes of m-SGO/EP nanocomposites
69x54mm (300 x 300 DPI)

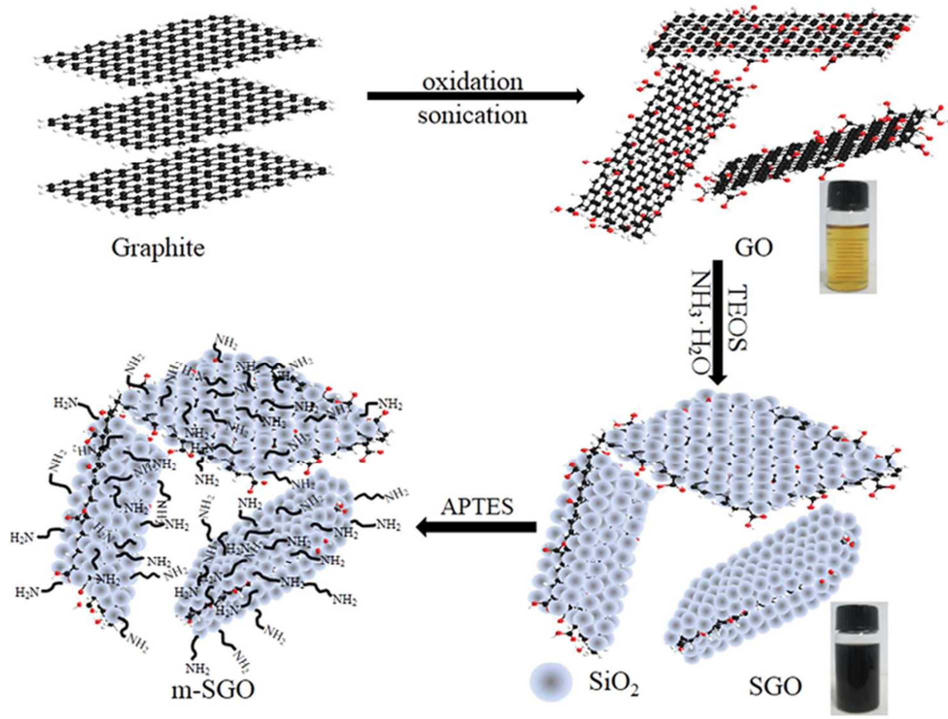

Scheme 1 Schematic illustration for the preparation of modified nanolsilica/graphene hybrid
88x88mm (300 x 300 DPI)

A novel nanosilica/graphene oxide hybrid and its flame retarding epoxy resin with simultaneously improved mechanical, thermal conductivities, and dielectric properties

Rui Wang[1], Dongxian Zhuo[1], Zixiang Weng[1], Lixin Wu[1*], Xiuyan Cheng[1], Yu Zhou[1], Jianlei Wang[1], Bowen Xuan[1]

A novel nanosilica/graphene oxide hybrid was successfully prepared, which can simultaneously improve the typical properties (dielectric, thermal conductivity, thermal stability, and mechanical properties) and flame retardancy of epoxy resin.